ADVANCED MATERIALS
www.advmat.de

Materials Views
www.MaterialsViews.com

Porphyrin-Tape/C_{60} Organic Photodetectors with 6.5% External Quantum Efficiency in the Near Infrared

By *Jeramy D. Zimmerman, Vyacheslav V. Diev, Kenneth Hanson, Richard R. Lunt, Eric K. Yu, Mark E. Thompson,* and *Stephen R. Forrest**

While few examples have been demonstrated, near-infrared (NIR) organic photodetectors with response at wavelengths (λ) beyond the cutoff of Si (i.e., $\lambda > 1100$ nm) are interesting for use in imaging and other detection applications.[1] In previous work, polymer photodetectors with response at $\lambda > 1000$ nm have been demonstrated, but the optical sensitivity is generally due to a long absorption tail having an external quantum efficiency (EQE) less than a few percent.[2–4] Organic materials systems with a large NIR photoresponse are rare for several reasons. A type-II (staggered) heterojunction must be formed between the donor and acceptor materials with a sufficient energy offset to dissociate photogenerated excitons; as the energy gap is decreased, finding molecular combinations with suitable energy alignments becomes increasingly difficult. In addition, exciton lifetimes generally decrease with energy gap due to exciton–phonon-induced recombination (i.e., internal conversion).[5,6] These difficulties have motivated the development of hybrid organic–inorganic devices using polymeric and small-molecule materials in conjunction with II–VI quantum dots (with EQE <1% at $\lambda > 1000$ nm)[7] or single-walled carbon nanotubes (EQE ≈ 2% at $\lambda = 1150$ and 1300 nm).[8] Here, we demonstrate an NIR EQE = 6.5% at $\lambda = 1350$ nm using photodetectors based on triply linked porphyrin-tape dimers. These porphyrin tapes are representative of a promising new class of materials that can be modified to exhibit even longer wavelength response by spatially extending the conjugation of the π-electron system.[5]

The molecules investigated consist of a base of two Zn-metallated porphyrins, triply linked at the *meso–meso* and both β–β positions, with four side groups of 3,5-di-*tert*-butylphenyl, but differ in the end terminations of singly bonded 4-cyanophenyl (CNPh), 3,5-di-*tert*-butyl-phenyl (DTBPh), pyrene (Psub), and doubly-bonded pyrene (Pfused) (see inset, **Figure 1**). The triply fused porphyrin tapes were synthesized as described previously.[9–11] Psub was converted to Pfused by a procedure similar to that reported by Osuka and co-workers.[12] The details of the synthesis of Psub and Pfused will be published elsewhere.[13] The compounds absorb throughout the visible and into the NIR with Q-band absorption peaks between wavelengths of $\lambda = 1050$ and 1350 nm, and have corresponding absorption coefficients of $\alpha = (1.5–3) \times 10^4$ cm^{-1}, as shown in Figure 1.

Films for materials characterization were deposited on bare, or poly(3,4-ethylenedioxythiophene)–poly(styrenesulfonate) (PEDOT–PSS)-coated quartz substrates using a film casting knife (i.e., a doctor blade). Atomic force microscopy (AFM) was used to measure surface morphology. CNPh was soluble (5–10 mg mL^{-1}) in pure chlorobenzene, and as shown in **Figure 2a**, formed large crystalline domains with a root mean square (RMS) roughness of >20 nm, which proved too rough for device fabrication. The addition of 1 vol% pyridine to CNPh enhanced its solubility, thereby decreasing the RMS roughness to 9.0 nm, and it changed the film morphology from large, cracked oak-leaf-shaped grains to almond-shaped grains as shown in Figure 2b. Both DBTPh and Psub were more soluble than CNPh (>10 mg mL^{-1}) in chlorobenzene, and formed films with 0.5 and 2.7 nm RMS roughness, respectively (Figure 2c,d). The solubility of Pfused was <2.5 mg mL^{-1} in chlorobenzene,

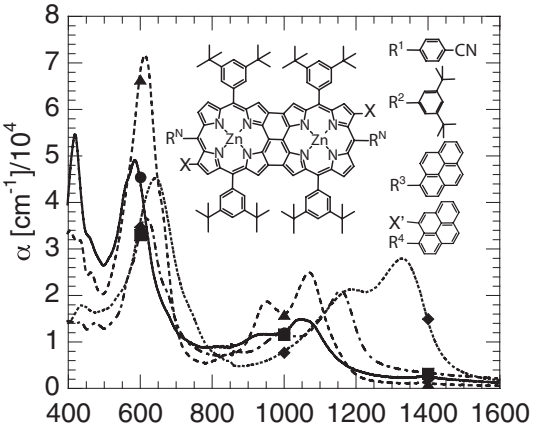

Figure 1. Absorption coefficients (α) of the four molecules studied: DTBPh, solid line (circles); CNPh, long-dashed line (squares); Psub, short-dashed line (triangles); and Pfused, dotted line (diamonds). Inset: Chemical structures of molecules studied. All donors use the same porphyrin-dimer base, and differ only in their end terminations. For CNPh, R = R^1 and X = H; for DTBPh, R = R^2 and X = H; for Psub, R = R^3 and X = H; and for Pfused, R = R^4 and X′ is the second bond to the pyrene.

[*] Dr. J. D. Zimmerman, R. R. Lunt, E. K. Yu, Prof. S. R. Forrest
Departments of Electrical Engineering and Computer Science
Materials Science and Engineering, and Physics
University of Michigan
Ann Arbor, MI 48109 (USA)
E-mail: stevefor@umich.edu
Dr. V. V. Diev, K. Hanson, Prof. M. E. Thompson
Department of Chemistry
University of Southern California
Los Angeles, CA 90089 (USA)
R. R. Lunt
Department of Chemical Engineering
Princeton University Princeton
NJ 08544 (USA)

DOI: 10.1002/adma.200904341

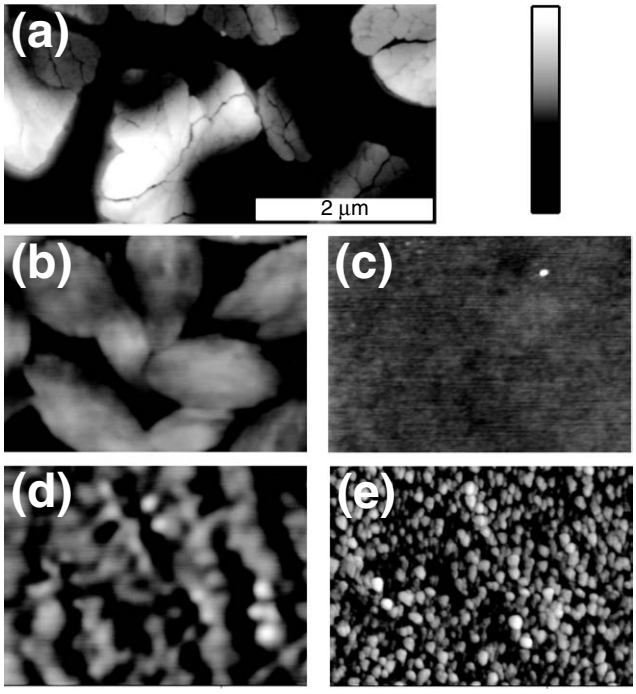

Figure 2. AFM images of films deposited by doctor blading a 0.5 wt/vol% solution in chlorobenzene of a) CNPh, b)CNPh with 1 vol% pyridine, c) DTBPh, d) Psub, and e) Pfused with 1% pyridine. The vertical scale range of the respective images are 110, 80, 20, 20, and 40 nm. The RMS roughnesses of the films are 20, 9.0, 0.5, 2.7, and 5.3 nm, respectively.

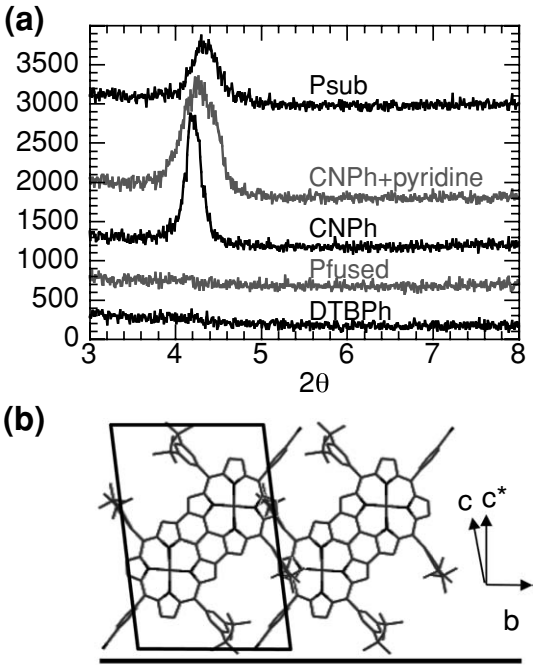

Figure 3. a) X-ray diffraction intensity of films consisting of the various porphyrin tape molecules indicated. b) Orientation of the molecules with respect to the substrate surface (black horizontal line). The (001) plane is parallel to the substrate surface; the projection of the (100) plane is shown by the parallelogram, and projections of the *b*- and *c*-directions of the unit cell are labeled. c^* denotes the direction perpendicular to the (001) plane and lies within the plane of the paper.

resulting in a thin (and hence overly transparent) film; the addition of 1 vol% pyridine increased solubility and resulted in films with a RMS roughness of 5.3 nm.

X-ray diffraction peaks (**Figure 3a**) were observed at $2\theta = 4.21 \pm 0.1°$ for CNPh cast from chlorobenzene, $4.28 \pm 0.1°$ for CNPh cast from chlorobenzene with 1 vol% pyridine, and $4.34 \pm 0.1°$ for Psub, corresponding to the distance between the (001) planes of 20.96 ± 0.50, 20.62 ± 0.48, and 20.32 ± 0.47 Å, respectively. These closely match the calculated (001) interplanar spacing of 20.2 and 20.0 Å for CNPh and Psub, respectively, as seen in the calculated crystal structure shown in Figure 3b. The lone (001) diffraction peak indicates that the molecules crystallize with their (001) planes parallel to the substrate surface. The addition of pyridine increases the full-width half-maximum (FWHM) of the CNPh diffraction peak from $0.214 \pm 0.004°$ (2θ) to $0.463 \pm 0.010°$ (2θ), corresponding to Scherrer broadening due to mean crystallite sizes of 43 ± 2 nm (~20 molecular layers) and 18 ± 1 nm (~9 molecular layers), respectively.[14] The FWHM for Psub is $0.354 \pm 0.010°$ (2θ), corresponding to a crystallite size of 24 ± 1 nm (~12 molecular layers). No diffraction peaks are observed for DTBPh or Pfused, indicating that the films are amorphous.

The reduction and oxidation potentials of Psub and Pfused were measured against a ferrocene/ferricinium reference. The reduction (oxidation) potentials for Psub and Pfused are –1.10 V (–0.01 V) and –0.97 V (–0.13 V), respectively. Reduction (oxidation) potentials for DTBPh, CNPh, and C_{60} have previously been measured at –1.07 V (+0.03 V), –1.07 V (+0.01 V), and –0.86 V, respectively.[15,16]

Devices were fabricated on precleaned PEDOT–PSS-coated indium tin oxide (ITO)-on-glass substrates using the same conditions as for the morphological studies, followed by sequential vacuum thermal evaporation (VTE) of C_{60}, bathocuproine (BCP), and the Ag cathodes (see Experimental section). Rectification ratios of $>2 \times 10^3$ at ±1 V were observed for CNPh, DTBPh, and Pfused, and $>2 \times 10^6$ for Psub devices. Ideality factors of $n \approx 1.3$ were observed for all devices except those based on CNPh, where $n \approx 1.8$, as shown in **Figure 4**. An ideality of $n < 1.5$ is typical of drift-diffusion, and an ideality between $n = 1.5$ and $n = 2$ is characteristic of defect-assisted generation-recombination in the bulk or at the donor–acceptor heterointerface. Defect-related traps may arise from the presence of impurities or morphological disorder.[17] When converting Psub to Pfused, the process of forming the additional bond to the pyrene end group reduces the reduction potential of Psub, therefore reducing the interfacial gap (i.e., the energy difference between the highest occupied molecular orbital, or HOMO, of the porphyrin tape molecule, and the lowest unoccupied molecular orbital, or LUMO, of C_{60}) by 0.12 eV, leading to a calculated 11-fold increase in interface-generated dark current,[18] compared with an observed difference of approximately three orders of magnitude. These differences suggest that an increased generation-recombination rate from defects is present in the CNPh and Pfused materials, as compared to DTBPh and Psub. Alternatively, the bulky end groups of Psub and DTBPh reduce the interaction between the donor and acceptor π-systems resulting in a reduced geminate

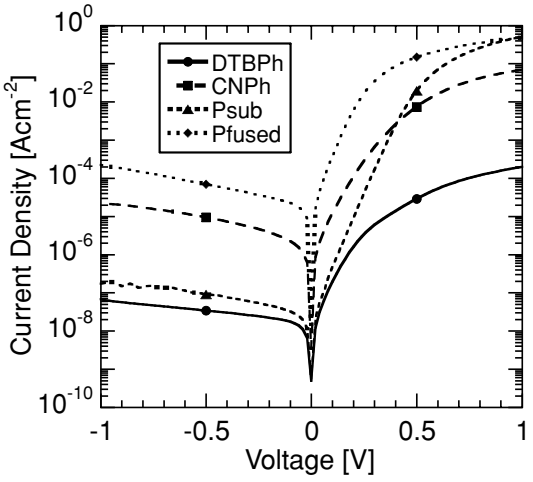

Figure 4. Current density versus voltage characteristics of the porphyrin tape/C_{60} photodetectors. Ideality factors and specific series resistances for detectors based on the several materials studied for DTBPh: $n = 1.31 \pm 0.11$ and $R_S = 530 \pm 160$ Ω cm; for CNPh: $n = 1.81 \pm 0.04$ and $R_S = 5.8 \pm 2.1$ Ω cm; for Psub: $n = 1.35 \pm 0.02$ and $R_S = 0.90 \pm 0.1$ Ω cm, and for Pfused: $n = 1.33 \pm 0.03$ and $R_S = 1.4 \pm 0.1$ Ω cm.

recombination and thus a lower dark current with respect to the CNPh and Pfused with the less bulky end groups.[19]

Spectrally resolved EQE for the several devices are shown in **Figure 5**. Peak efficiencies of 1.2 ± 0.1%, 1.6 ± 0.1%, 2.1 ± 0.1%, and 6.5 ± 0.3% at wavelengths of λ = 1045, 1130, 1090, and 1345 nm are observed for DTBPh-, CNPh-, Psub-, and Pfused-based devices, respectively. A transfer matrix model was used to determine the internal quantum efficiency (IQE) from the EQE data and the optical properties of the device structures.[20] In a structure consisting of a 20 ± 4 nm thick film of Pfused, 125 nm of C_{60}, 10 nm of BCP, and 100 nm of Ag, 19 ± 5% of the incident radiation at λ = 1350 nm light is absorbed, while the observed EQE was 5.9%. This results in IQE = 31 ± 8%, indicating that excitons are collected from an active region thickness of 6.2 ± 1.6 nm. Films cast from solutions of 0.25, 0.5, and 1 mg mL^{-1} in chlorobenzene resulted in thicknesses of 20 ± 4, 60 ± 12, and 120 ± 24 nm, resulting in EQE = 5.3 ± 0.6%, 6.2 ± 0.4%, and 4.5 ± 0.4% at λ = 1350 nm, respectively. The weak dependence on donor-layer thickness is consistent with a diffusion length smaller than the thinnest film.

The specific detectivity is calculated using: $D^* = RA^{1/2}S_N^{-1}$, where R is the responsivity, A is the detector active area, and S_N is the RMS noise current spectral density.[21] Peak specific detectivities at zero bias, where thermal noise dominates,[21] of $D^* = (1.6 \pm 0.1) \times 10^{11}$ Jones at $\lambda = 1090$ nm for Psub-, and $(2.3 \pm 0.1) \times 10^{10}$ Jones at $\lambda = 1350$ nm for Pfused-based devices were obtained, as shown in Figure 5. These detectivities are significantly less than for InGaAs detectors (~10^{13} Jones) that are sensitive within the same wavelength range, but are comparable to those obtained using cooled PbS detectors.[1,22]

The electrical response to optical excitation using an external 50 Ω load was used to probe photogenerated carrier extraction and device bandwidth, with results shown in **Figure 6**. For Psub-based detectors, the response decay time constant is $\tau = 2.09 \pm 0.02$ ns at $V = 0$, decreasing asymptotically to $\tau = 1.87 \pm 0.03$ ns at −1 V. This corresponds to 3 dB roll-off frequency of 56 ± 7 MHz as shown in the inset of Figure 6. At −1 V, the response times of Pfused-, DTBPh-, and CNPh-based devices are $\tau = 2.15 \pm 0.02$, 2.30 ± 0.02, and 3.17 ± 0.02 ns, respectively. The capacitances of the devices are between C = 20.4 and 21.6 nF cm^{-2}, indicating fully depleted active regions that should have resistance–capacitance (RC) time constants of ~0.8 ns across a 50 Ω load, assuming series resistance is negligible. Here, τ was found to decrease when either the C_{60} and/or the porphyrin layer thickness was increased, thus decreasing capacitance, indicating that parasitic series resistance introduces a limit to the device bandwidth.

In conclusion, we have demonstrated that porphyrin tape molecules are promising for use in NIR photodetector applications. By extending the conjugation length in this broad class of materials, the absorption is extended from the near visible to

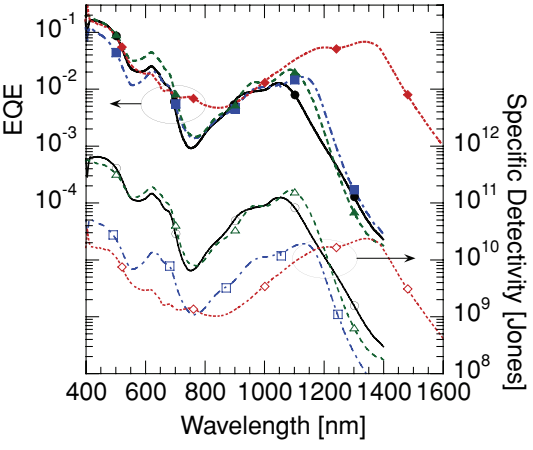

Figure 5. External quantum efficiencies of devices fabricated from the several porphyrin tape compounds are shown with heavy lines (upper set). Specific detectivity of the same devices are show with the lighter lines (lower set). Line types are DTBPh, solid; CNPh, dotted-dashed; Psub, dashed; and Pfused, dotted.

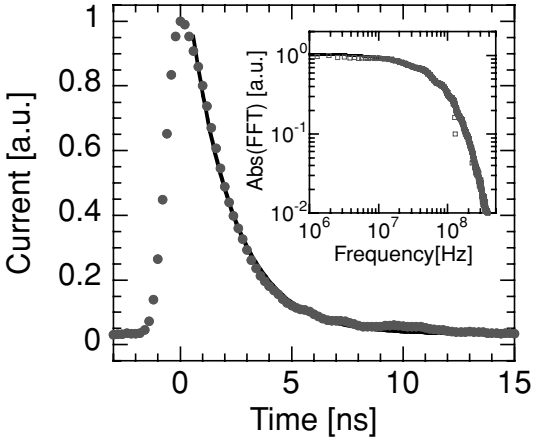

Figure 6. Electrical response of a 0.3 mm diameter device biased at −1 V using a 1 ns pulse at λ = 1064 nm. The fit corresponds to a decay time constant of 1.87 ± 0.03 ns. Inset: Bode plot of the electrical response, indicating a 3 dB roll-off frequency of 56 ± 7 MHz.

deep into the NIR. The detector performance is influenced by the functionalizing substituent molecule that, in turn, affects the film crystal structure and morphology. Detectors based on Pfused, have a peak EQE = 6.5%, $D^* = (2.3 \pm 0.1) \times 10^{10}$ Jones, and a response time of $\tau = 2.12 \pm 0.02$ ns at $\lambda = 1350$ nm.

Experimental Section

Sample Fabrication: Devices were fabricated on glass substrates with a 150 nm thick layer of ITO predeposited on their surfaces. Prior to organic film deposition, the substrates were cleaned in Tergitol, trichloroethylene, acetone, and isopropanol followed by a 15 min anneal at 300 °C in air to increase transparency.[8] Next, a 25 ± 5 nm thick layer of PEDOT–PSS was spun-on and baked at 125 °C for 10 min on a hotplate to improve substrate planarity. The substrates were then transferred to a N_2 glovebox (O_2 and H_2O <1 ppm) where layers of porphyrin dimers were deposited at 120 °C with a doctor blade. It was found that for all molecules ~0.5 wt% solutions in chlorobenzene provided the highest EQE. Subsequently, an 80–125 nm thick layer of C_{60} followed by a 10 nm thick BCP layer were deposited by vacuum thermal evaporation in a chamber with a base pressure of 10^{-7} torr. The active device area was defined by depositing a 100 nm thick Ag cathode through a shadow mask with arrays of 1 and 0.3 mm holes. Errors in determining the thicknesses of evaporated layers by spectroscopic ellipsometry are typically <5%. Samples for materials investigations were deposited using the same procedures on bare or PEDOT–PSS-coated quartz. A 0.5 mg mL^{-1} solution formed ~50 ± 15 nm thick films. Materials used were PEDOT–PSS (H.G. Stark, Cleavios P), C_{60}(Alfa Aesar, sublimed grade, additionally purified once by thermal gradient sublimation), and BCP (Luminescent Technologies Inc).

Device Electrical and Optical Measurements: Current versus voltage characteristics were measured using a HP 4156C semiconductor parameter analyzer. The EQE was measured using ~200 Hz chopped light from a monochromated 1000 W tungsten lamp coupled to the device using an optical fiber. A set of long pass filters was used to eliminate diffraction orders (m) greater than $m = 1$. The spectral resolution of the measurement is approximately 10 nm. Optical power was calibrated using Newport 818-series NIST-traceable Si and Ge photodetectors, and was between 1 and 10 μW over the wavelength range tested. Device and reference photodetector currents were measured using a Stanford Research Systems SR830 DSP lock-in amplifier. Speed of response was measured on 0.3 mm diameter devices with $\lambda = 1064$ nm emission from a diode-pumped yttrium aluminum garnet laser with a pulse width of ~1 ns and a repetition rate of 6.6 kHz. Samples were biased using a bias-T and a source meter.

Materials Characterization: Film morphology and thickness were characterized using a Nanoscope III atomic force microscope in the tapping mode, a Perkin Elmer 1050 spectrophotometer for absorbance measurements, and a Rigaku X-ray diffractometer in the Bragg–Brentano configuration using a rotating anode producing Cu-Kα radiation for diffraction measurements. The error in diffraction angle (±0.1°) is due to uncertainty in sample placement on the stage.

Crystal Structure Calculations: Crystal structures were calculated using the Forcite module in Material Studio v4.4 with the Universal force field parameterization with a cutoff distance of 50 Å. The calculated crystal structures are all triclinic, space group P: DTBPh, $a = 9.42$ Å, $b = 16.97$ Å, $c = 20.92$ Å, $\alpha = 72.81°$, $\beta = 85.78°$, and $\gamma = 77.47°$; CNPh, $a = 9.78$ Å, $b = 13.23$ Å, $c = 21.22$ Å, $\alpha = 85.86°$, $\beta = 71.89°$, and $\gamma = 72.45°$; Psub, $a = 9.77$ Å, $b = 14.79$ Å, $c = 21.29$ Å, $\alpha = 86.42°$, $\beta = 69.88°$, and $\gamma = 76.58°$.

Optical Model: A transfer matrix model was used to calculate the optimum C_{60} thickness and the light absorbed by the Psub device.[20] The thicknesses of each layer matched those in the devices tested: 10 nm BCP, 125 nm C_{60}, 20 ± 4nm Pfused, 25 nm PEDOT–PSS, and 150 nm ITO. The real and imaginary indices of refraction for Pfused at $\lambda = 1350$ nm are $n = 1.9$ and $\kappa = 0.30 \pm 0.06$.

Acknowledgements

The authors thank C. K. Renshaw and S. Kéna-Cohen for useful discussions, and the Defense Advanced Research Projects Agency HARDI Program and Universal Display Corp. for their partial financial support. The views, opinions, and/or findings contained in this article/presentation are those of the author/presenter and should not be interpreted as representing the official views or policies, either expressed or implied, of the Defense Advanced Research Projects Agency or the Department of Defense.

Received: December 17, 2009
Revised: February 4, 2010
Published online: April 19, 2010

[1] A. Rogalski, *Infrared Phys. Technol.* **2002**, *43*, 187.
[2] Y. J. Xia, L. Wang, X. Y. Deng, D. Y. Li, X. H. Zhu, Y. Cao, *Appl. Phys. Lett.* **2006**, *89*, 081106.
[3] L. Wen, B. C. Duck, P. C. Dastoor, S. C. Rasmussen, *Macromolecules* **2008**, *41*, 4576.
[4] E. Perzon, F. L. Zhang, M. Andersson, W. Mammo, O. Inganas, M. R. Andersson, *Adv. Mater.* **2007**, *19*, 3308.
[5] H. S. Cho, D. H. Jeong, S. Cho, D. Kim, Y. Matsuzaki, K. Tanaka, A. Tsuda, A. Osuka, *J. Am. Chem. Soc.* **2002**, *124*, 14642.
[6] D. Tittelbachhelmrich, R. P. Steer, *Chem. Phys.* **1995**, *197*, 99.
[7] X. M. Jiang, R. D. Schaller, S. B. Lee, J. M. Pietryga, V. I. Klimov, A. A. Zakhidov, *J. Mater. Res.* **2007**, *22*, 2204.
[8] M. S. Arnold, J. D. Zimmerman, C. K. Renshaw, X. Xu, R. R. Lunt, C. M. Austin, S. R. Forrest, *Nano Lett.* **2009**, *9*, 3354.
[9] A. Tsuda, H. Furuta, A. Osuka, *Angew. Chem. Intl. Ed.* **2000**, *39*, 2549.
[10] M. Kamo, A. Tsuda, Y. Nakamura, N. Aratani, K. Furukawa, T. Kato, A. Osuka, *Org. Lett.* **2003**, *5*, 2079.
[11] F. Y. Cheng, S. Zhang, A. Adronov, L. Echegoyen, F. Diederich, *Chem. Eur. J.* **2006**, *12*, 6062.
[12] K. Kurotobi, K. S. Kim, S. B. Noh, D. Kim, A. Osuka, *Angew. Chem. Intl. Ed.* **2006**, *45*, 3944.
[13] V. V. Diev, K. Hanson, M. E. Thompson, unpublished.
[14] A. Guinier, *X-ray Diffraction in Crystals, Imperfect Crystals, and Amorphous Bodies*, W.H. Freeman, San Francisco, CA **1963**.
[15] L. A. Fendt, H. Fang, M. E. Plonska-Brzezinska, S. Zhang, F. Cheng, C. Braun, L. Echegoyen, F. Diederich, *Eur. J. Org. Chem.* **2007**, *28*, 4659.
[16] S. A. Lerke, B. A. Parkinson, D. H. Evans, P. J. Fagan, *J. Am. Chem. Soc.* **1992**, *114*, 7807.
[17] N. Li, B. E. Lassiter, R. R. Lunt, G. Wei, S. R. Forrest, *Appl. Phys. Lett.* **2009**, *94*, 023307.
[18] B. P. Rand, D. P. Burk, S. R. Forrest, *Phys. Rev. B* **2007**, *75*, 115327.
[19] M. D. Perez, C. Borek, S. R. Forrest, M. E. Thompson, *J. Am. Chem. Soc.* **2009**, *131*, 9281.
[20] P. Peumans, A. Yakimov, S. R. Forrest, *J. Appl. Phys.* **2003**, *93*, 3693.
[21] S. M. Sze, *Physics of Semiconductor Devices*, John Wiley and Sons, New York **1981**, xii.
[22] J. G. Webster, *The Measurement, Instrumentation, and Sensors Handbook*, CRC Press in cooperation with IEEE Press, Boca Raton, FL **1999**.